# Dynamics and Size of Cross-Linking-Induced Lipid Nanodomains in Model Membranes

Martin Štefl,[†] Radek Šachl,[†‡] Jana Humpolíčková,[†] Marek Cebecauer,[†] Radek Macháň,[†] Marie Kolářová,[†] Lennart B.-Å. Johansson,[‡] and Martin Hof[†]

[†]Department of Biophysical Chemistry, J. Heyrovsky Institute of Physical Chemistry of the Academy of Sciences of the Czech Republic, Dolejškova, Prague, Czech Republic; and [‡]Department of Chemistry: Biophysical Chemistry, Umeå University, Umeå, Sweden

**Supporting Information**

*Two-color z-scan FCS*

Z-scan FCS is a calibration-free FCS method which allows for precise determination of diffusion coefficients in planar systems.[1] The principle of z-scan FCS is based on acquiring individual fluorescence intensity traces at different positions of the planar system (bilayer) with respect to the optical axis (z-axis) of the focal volume. The intensity traces $I(t)$ obtained at every position are individually correlated according to the formula:

$$G(\tau) = \frac{\langle I(t) I(t+\tau) \rangle}{\langle I(t) \rangle^2}, \qquad \text{Eq. 1}$$

where the angle brackets represent temporal averaging. Resulting autocorrelation functions are subsequently fit with suitable model. In our case, we have applied two-dimensional Brownian diffusion model assuming Gaussian point spread function (PSF). The theoretical shape of the autocorrelation function $G(\tau)$ is described by:

$$G(\tau) = 1 + \left[ 1 - T + T e^{\frac{-\tau}{\tau_T}} \right] \frac{\gamma}{N(1-T)} \frac{1}{1 + \frac{\tau}{\tau_D}}, \qquad \text{Eq. 2}$$

where $T$ corresponds to a fraction of fluorophores in the triplet state, $\tau_T$ is a parameter characterizing the triplet state transition, $\gamma$ is a factor accounting for beam geometry ($\gamma = ½$ for 2D), $N$ stands for average number of particles in the illuminated spot and $\tau_D$ is the transition time, i.e. the time the molecule needs to pass through the illuminated area. When fitting our data $T$, $\tau_T$, $N$, and $\tau_D$ were free parameters. Since the triplet fraction is usually small (~ 5 %) if any and $\tau_T$ is in μs-time range, these two parameters do not have a significant impact for the fit. Due to Loretzian character[2] of intensity profile in the tightly focus laser beam, the read-out parameters $\tau_D$ and $N$ plotted versus the position of the bilayer with respect to the laser focus $z$ follow the equations:

$$\tau_D(z) = \frac{\omega_0^2}{4D} \left( 1 + \frac{\lambda^2 (z - z_0)^2}{n^2 \pi^2 \omega_0^4} \right), \qquad \text{Eq. 3}$$

$$N(z) = \pi c_s \omega_0^2 (1 + \frac{\lambda^2 (z - z_0)^2}{n^2 \pi^2 \omega_0^4}), \qquad \text{Eq. 4}$$

where $\omega_0$ is the radius of the waist of the laser focus, $\lambda$ is excitation wavelength, $n$ stands for refractive index, $D$ is a diffusion coefficient, $z_0$ is the $z$-coordinate corresponding to the situation when the bilayer is in the waist of the laser beam, and $c_s$ is planar concentration of diffusing molecules. When fitting the parabolas to the measured $\tau_D$- and $N$-dependences, $D$, $c_s$, and $\omega_0$ are free parameters.

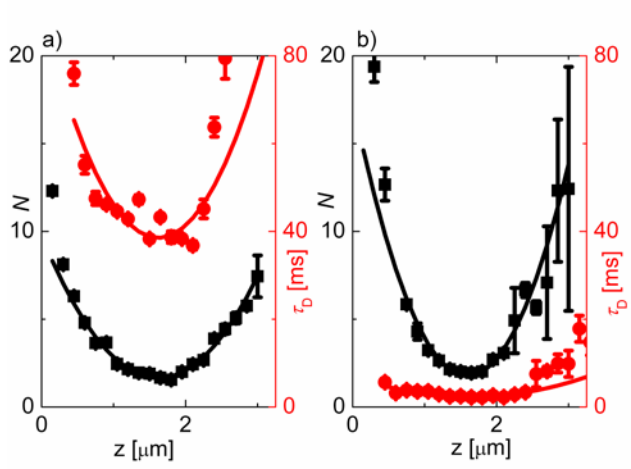


Figure S1. Dependence of the particle number (black) and the mean transition time (red) on the relative position of a bilayer with respect to the optical axis for CTxB-647 (a) and BDP-DHPE (b) measured in the upper GUV membrane composed of lipid mixture **B** at high crosslinker load.

A typical example of the two color z-scan experiment is depicted in Fig. S1. In this particular example, intensity fluctuations of CTxB-647 (high loaded composition **B**) and BDP-DHPE were simultaneously acquired and processed as described above. Particle number and the transition time dependences for both the dyes show the expected parabolic behavior. When fitting the parabolas with models given by Eg. 3 and Eq. 4, the diffusion coefficient (or apparent diffusion coefficient if the diffusion is not free) and surface concentration can be withdrawn.

*Diffusion law and its application in z-scan FCS*

Wawrezinieck *et al* studied the dependence of the mean transition time through the

illuminated area on the area size.[3] Due to the fact that in optical microscopy the minimum size of the illuminated area is diffraction limited and that the expected diffusion barriers such as rafts or cytoskeleton meshwork are much smaller than the limit, Monte Carlo simulations were employed. The particular type of the barriers was generated and the apparent transition times simulated as a function of the area size. The dependence is linear if the structures of interest are much smaller compared to the illuminated spot and follow the so called "diffusion law":

$$\tau_D^{app} = t_0 + \frac{\omega^2}{4D_{eff}}. \qquad \text{Eq. 5}$$

$\tau_D^{app}$ is the time a molecule passes through the detection area, $\omega$ stands for the spot radius, $D_{eff}$ is an effective diffusion coefficient which bears the information about the barrier-free diffusion coefficient, probability of crossing the barriers and the density of membrane structures (in the case of isolated domains). The intercept $t_0$ is equal to zero for homogeneous membranes, negative in the case of meshwork, and positive in presence of isolated domains in the membrane. With knowledge of the diffusion coefficient in a homogenous membrane $D_{free}$ and $D_{eff}$ determined from Eq. 5, the time based partition coefficient $\alpha$ (fraction of time a molecule spends in the domains) can be calculated:

$$D_{eff} = (1-\alpha)D_{free}. \qquad \text{Eq. 6}$$

The intercept $t_0$ is related to the confinement time, i.e. the time a molecule is trapped in the domain, $\tau_{\text{conf}}$ and the time the molecule diffuses from the center of the domain to its boundary $\tau_D^{domain}$:

$$t_0 = 2\alpha(\tau_{conf} - \tau_D^{domain}). \qquad \text{Eq. 7}$$

Usually, it is assumed that $\tau_{conf} \gg \tau_D^{domain}$.

Since the illuminated spot size is being inherently changed during the z-scan, and the number of particles serves as a measure of the size, the diffusion law can be constructed from the z-scan FCS data as introduced by Humpolíčková *et al.*[4] Eq. 6 is extended as follows:

$$\tau_D^{app} = t_0 + \frac{\omega_0^2}{4D_{eff}} \frac{N}{N_0}. \qquad \text{Eq. 8}$$

Fig. 3 in the manuscript shows dependences of the CTxB-647/BDP-DHPE transition time on the $N/N_0$ ratio for selected GUVs at investigated compositions. Table S1 gives values of intercepts and slopes of the given dependences obtained by linear fitting.

| Species/Composition | Intercept | Error | Slope | Error |
|---|---|---|---|---|
| | [ms] | [ms] | [ms] | [ms] |
| BDP-DHPE/**B**(high load) | -0.9 | 0.6 | 3.1 | 0.5 |
| CTxB-647/**A** | 0.6 | 0.9 | 5.0 | 0.8 |
| CTxB-647/**B**(low load) | 2.5 | 2.8 | 3.5 | 2.5 |
| CTxB-647/**B**(high load) | 54.9 | 7.3 | 26.1 | 4.9 |
| CTxB-647/**C** | -0.6 | 2.8 | 13.2 | 2.3 |

Table S1. Intercepts and slopes for the linear $\tau_D^{app} \sim N/N_0$ dependences given in Fig. 3.

*Relative brightness of CTxB-647 labeled clusters and two-color cross-correlation experiments*

To better understand the source of long transition times observed for the highly loaded **B**-composed GUVs, relative brightness of CTxB-647 clusters, i.e. number of photons generated by a single cluster per second, was estimated for every concentration of the crosslinker. We assume that changes in relative brightness would roughly correspond to the clustering degree, i.e. refer to the average number of CTxB- 647-GM1 pentamers in a nanodomain. The results are shown in Table S2.

| composition **B**, CTxB-647 load | low | medium | high |
|---|---|---|---|
| relative brightness [kHz/molecule] | 2.2 | 3.1 | 5.0 |
| SD | 0.5 | 0.7 | 1.7 |
| n | 4 | 4 | 4 |
| relative average aggregation number | 1.0 | 1.4 | 2.2 |

Table S2. Relative brightness of CTxB-647 clusters obtained from z-scan FCS experiments performed on **B**-composed liposomes for different crosslinker concentrations. *SD* stands for a standard deviation, and *n* is a number of z-scans acquired.

The relative brightness $\beta$ was calculated as follows: $\beta = counts/N$ , where "counts" is the average countrate in the red detection channel arising upon excitation with the red laser, $N$ is a number of particles obtained from amplitude of ACF. The relative brightness changes with the position of the bilayer with respect to the focused beam giving a distinct maximum when the bilayer is in the focus. The maximal values are those used in Table S2.

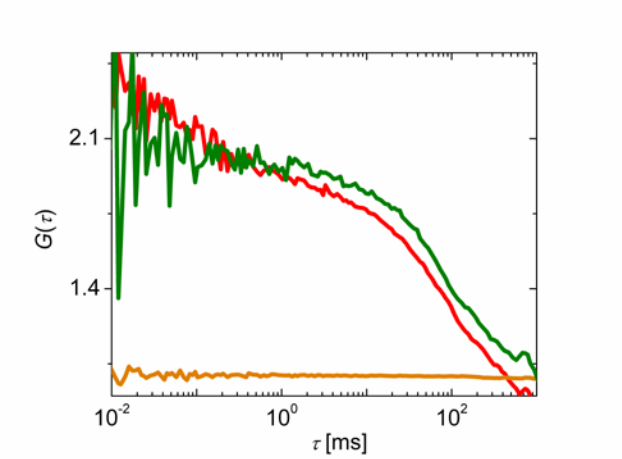


Figure S2. ACFs for CTxB-647 (red curve) and CTxB-488 (green curve) acquired in two-color z-scan FCS experiment performed in upper membrane of **B**-composed GUVs. Orange curve is a cross-correlation function between the red and green dignal. The curves shown correspond to the situation when membrane is in the laser focus.

In order to understand whether the assemblies revealed in the given brightness analyses are solid patches coupling the motion of individual CTxB-647 particles together, liposomes were treated with an equimolar mixture of CTxB-647 and CTxB-488 and the cross-correlation between the red and green signal was investigated (see Fig. S2). The fact that no cross-correlation appears indicates uncoupled motion of CTxB-GM1

complexes, which supports our assumption that the nanodomains result from lipid-lipid interactions rather than mutual interactions between the crosslinker molecules.

*Phasor approach in FLIM-FRET analysis*

Phasor plot is a graphical, non-fitting approach for visualization of different fluorescence decay functions in FLIM images.[5] In our experiments, phasor plots were used to characterize changes in donor decays in a FRET experiment. Fig. S3 shows an example of a GUV formed by lipid mixture **D**. This example is used to demonstrate the data treatment applied to our FLIM-FRET data.

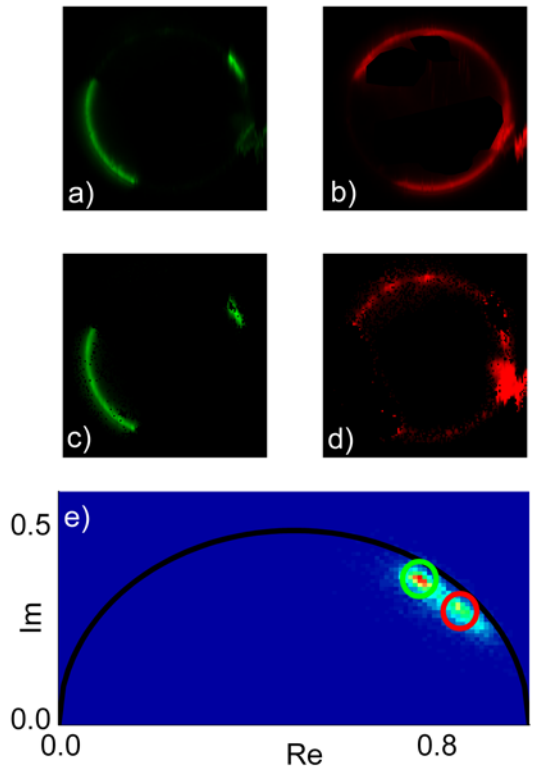


Figure S3. a) and b): intensity images of CTxB-488 and DiD measured for a GUV formed by the lipid mixture **D**. c) and d) depicts pixels corresponding to the different decay functions of CTxB-488 observed in the phasor plot (e).

For the FRET experiments, GUVs were labeled with DiD, acceptor molecules, residing in the $L_d$ phase. The donor molecule, CTxB-488, binds to gangliosides GM1

preferentially occupying the $L_o$ phase. Acquisition of every image is done using two-color, pulse-interleaved excitation (470 and 640 nm) and the fluorescence signal is split on two detectors, therefore simultaneously measured intensity images of the donor and the acceptor can be reconstructed (Fig. S3a and S3b). At every pixel of the image, the decay histogram is acquired using time-correlated single photon counting (TCSPC). The resulting 3D matrix is converted to the phasor diagram in the following way:

i) For every pixel, the phasor plot coordinates are calculated using formula:

$$\begin{bmatrix} \mathrm{Re} \\ \mathrm{Im} \end{bmatrix} = \frac{1}{\sum_{i=1}^{L} I_i} \begin{bmatrix} \sum_{i=1}^{L} I_i \cos\frac{2\pi n}{L}(i - i_0) \\ \sum_{i=1}^{L} I_i \sin\frac{2\pi n}{L}(i - i_0) \end{bmatrix}, \qquad \text{Eq. 9}$$

$I_i$ is fluorescence intensity in the $i$-th TCSPC channel, $L$ stands for the number of TCSPC channels, $n$ is an arbitrarily chosen integer (here $n$ = 4) corresponding to the frequency in the Fourier space, $i_0$ is a channel position of the decay rising edge. $i_0$ is commonly determined by measuring TCSPC histogram of a single exponential dye (fluorescein). Its value is being varied as long as the position of the single exponential decay in the phasor diagram lies on the universal circle (black line in Fig. S3e).

ii) 2D histogram of the phasor plot coordinates is constructed (Fig. S3e). Clusters in the phasor plot correspond to various spatially resolvable decay functions. The two clusters in Fig.S3e are assigned to the pixels with higher FRET (red circle in Fig. S3e and Fig. S3d) and the lower FRET contribution (green circle in Fig. S3e and Fig. S3c). Figure S3 proves that the lower FRET is observed in the $L_o$ phase while higher contribution of energy transfer corresponds to the $L_d$ phase. If the phases are not spatially resolvable, every pixel contains both low and high FRET contributions, which results in a single cluster in the phasor plot.

Fig. 4 in the manuscript gives only peak positions of individual lifetime clusters, the entire phasor plots for CTxB-488 donor lifetime in GUVs are given in Fig. S4:

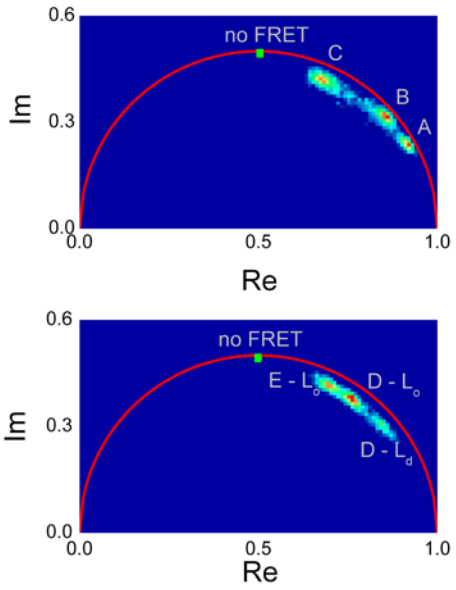


Figure S4. Positions of CTxB-488 donor decay clusters in the phasor plot for GUVs composed of lipid mixture A to C (upper part), and D to E (lower part). Position of a decay corresponding to no FRET is marked. No FRET decay was measured in solution containing CTxB-488.

*Baumann-Fayer model*

Baumann-Fayer[6] model accounts for energy transfer/migration within one leaflet of the bilayer in a two-dimensional geometry, or between two parallel planes separated from each other at distance *d*. According to the model, the energy transfer contributes to the fluorescence decay $F(t)$ of a donor according to:

$$F(t) = G^s(t)\sum_i \alpha_i \exp\left(-\frac{t}{\tau_i}\right) \qquad \text{Eq. 10}$$

In Eq. 10, $\alpha_i$ and $\tau_i$ describe the donor fluorescence in the absence of acceptors. The function $G^s(t)$ stands for the probability that a donor initially excited at $t = 0$ is still excited at time $t$ later. In a lipid bilayer where both D and A reside at the interface of the bilayer excited energy can be transferred to either A localized in the same leaflet, this

process is described by the intra-layer probability $G^{s}_{intra}(t)$, or to an acceptor localized in the opposite leaflet. This event is then described by an inter-layer probability $G^{s}_{inter}(t)$. The total probability $G^{s}(t)$ is given by the joint probability $G^{s}(t) = G^{s}_{intra}(t)G^{s}_{inter}(t)$. For isotropically oriented donor and acceptors which reorient fast as compared to the rate of energy transfer (*i.e.* the dynamic limit condition), $G^{s}_{intra}(t)$ is given by

$$\ln G^{s}_{intra}(t) = -C_2 \Gamma(2/3)(t/\tau)^{1/3} \qquad \text{Eq. 11}$$

Here $C_2$ is a so called reduced concentration corresponding to the average number of acceptors within a circle limited by the Förster radius of the donor ($R_0$) and $\Gamma$ is the gamma function. The probability of inter-leaflet energy transfer is given by

$$\ln G^{s}_{inter}(\mu) = -\frac{C_2}{3}(d/R_0)^2 (2\mu/3)^{1/3} \int_0^{2/3\mu} (1-e^{-s}) s^{-4/3} ds \qquad \text{Eq. 12}$$

In Eq. 12, $d$ is the distance between the leaflets where the chromophores reside, $\mu = 3t(R_0/d)^6/2\tau$ and $s = 2\mu\cos^6\theta_r/3$, where $\theta_r$ denotes the angle between the bilayer normal and the vector $\boldsymbol{r}$ which connects the locations of the donor and acceptor dipoles.

*Monte Carlo simulations*

Analytical equations describing FRET exist for a limited number of basic geometries and are quite complex and not easy to derive. Therefore it is convenient to apply Monte Carlo simulations, which successively mimic various random processes. Here we have used this technique to simulate FRET in a lipid bilayer containing circular nanodomains. The following steps have been carried out: (i) A certain number of domains corresponding to a pre-defined area occupied by the domains was generated. (ii) Donors and acceptors were distributed with a certain probability of being localized within and outside the domains. The distribution is described by an equilibrium constant ($K_{D,A}$ = [donors (acceptors) within]/[donors (acceptors) outside]). (iii) A donor was randomly excited and assumed to transfer its excitation energy to an acceptor, which was localized either in the same plane or in the opposite leaflet. The time $\Delta t_i$ elapsed from the excitation to the transfer event depends on the overall energy transfer rate $\Omega_i$ according to:

$$\Delta t_i = -\frac{\ln \alpha}{\Omega_i}, \qquad \text{Eq. 13}$$

where $\alpha$ denotes a random number between 0-1. The total energy transfer rate is calculated as a sum of energy transfer rates from the excited donor *i* to all acceptors. Acceptors that are beyond the cut-off distance $10\,R_0$ are included via the continuum approach (periodic boundary):

$$\Omega_i = \sum_j \frac{3}{2}\kappa_{ij}^2 \left(\frac{R_0}{R_{ij}}\right)^6 \tau_D^{-1} + C_2 \left(\frac{R_0}{R_C}\right)^4 \tau_D^{-1}, \qquad \text{Eq. 14}$$

Here *j* goes from 1 to the number of acceptors found within the cut-off distance $R_C$. $R_{ij}$ is the distance between the *i*-th donor and *j*-th acceptor, $R_0$ the Förster radius, $\tau_D$ lifetime of the donor in the absence of any acceptor and $\kappa_{ij}^2$ is the so called kappa factor. The second term in Eq. 14 accounts for rates between the excited donor and the continuum of acceptors exceeding the donor-acceptor distance $R_C$ distributed over two parallel planes.[7] Due to 1/6 power dependence of FRET rate efficiency on *R* and rather large size of the replicated box ($10\,R_0 \times 10\,R_0$) this term constitutes negligibly to $\Omega$. New configurations were generated approximately 3000 times and each generated configuration set was 100 times excited and used in the calculation step (iii). The outcome of the simulation is the $G(t)$ function , which is related to the fluorescence decay via B-F model (Eq. 10). The generated decay was then fitted to the experimental one by changing the variable input parameters, the domain radius and the area occupied by the domains. The remaining parameters were fixed: $R_0$ = 5.4 nm, $K_D$, $K_A$, reduced surface concentration $C_2$ obtained from the B-F model, parameters $A_i$ and $\tau_i$ of the donor decay in the absence of acceptors and the bilayer thickness $d$ = 38 Å.[8]

*Perylene-to-DiD energy transfer and changes in perylene lifetime*

To support our hypothesis that while in the composition **B**, the domain formation is initiated by the crosslinker, in the composition **C**, the domains are formed already prior crosslinker addition, we have measured lifetime of perylene (donor) in GUVs formed of the lipid mixture **B** and **C** in the presence of DiD (acceptor) before and after addition of the non-labeled crosslinker (CTxB). The distribution constant *K* of perylene between the

liquid-ordered and liquid-disordered phase was estimated to be around 0.8 (intensity image of phase separated GUV formed of the mixture **D** was analysed, $K$ was calculated as: $K = \left(I\left(\mathrm{L_o}\right)\tau\left(\mathrm{L_d}\right)\right)/\left(I\left(\mathrm{L_d}\right)\tau\left(\mathrm{L_o}\right)\right)$, where $I$ and $\tau$ are average pixel intensities and lifetimes of perylene, respectively, in the given phase). Additionally, perylene has a longer lifetime in the $L_o$ phase (7-8 ns) than in the $L_d$ phase (5.5-6 ns). Thus, when nanodomains are formed, certain perylene fraction becomes separated from the acceptor, which results in longer average lifetime first, due to lower FRET and second, due to occupation of the $L_o$ phase. Changes in fluorescence decay profiles are depicted in Fig. S5.

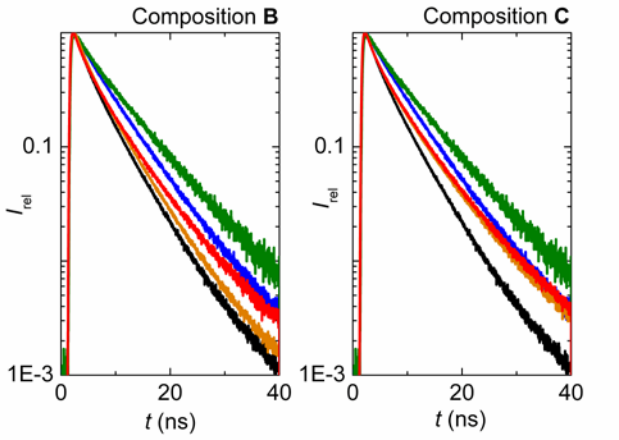


Fig. S5. Fluorescence decay profile of perylene in GUVs formed of lipid mixture **B** (left) and **C** (right) before (orange) and after (red) addition of CTxB. For comparison, perylene decays in the composition **A** without (blue) and with (black) acceptor are given as well as the perylene decay in the $L_o$ phase of the **D** composed GUVs (green). The experimental conditions were the same as were used for the CTxB-488-to-DiD FRET measurements except from the fact that no labeled CTxB was added and instead perylene was present in label-to-lipid ratio 1:200.

The figure shows that in the liposomes composed of the mixture **B**, the donor decay resembles the decay in the composition **A** when both donors and acceptor are homogeneously distributed in the Sph- free membrane. When CTxB is added, perylene decay starts to deviate towards longer lifetimes typical for the $L_o$ phase. In contrast, in

the composition **C**, the longer decay component is present already before adding of the crosslinker and after its addition almost no decay change was detected.

We are aware of the fact that the decay of perylene is subjected not only to presence of FRET and phase it resides, but it also reflects lipid composition and cholesterol content. In addition, it tends to dimer/excimer formation that may cause additional energy transfers.[9] Therefore, in this work, we did not apply the MC simulations as we did in the case of CTxB-488-to-DiD FRET and restrict ourselves to qualitative data interpretation.

*Calculation of collision rates*

In order to explain the crosslinker concentration dependence of the diffusion characteristics observed for the **B** composed membranes, we propose the following model: at low CTxB-647 load, gangliosides GM1 are pentamerized, forming a sphingomyelin-stabilized disks that diffuse freely with a diffusion coefficient $D = 2.6$ $\mu m^2 s^{-1}$, which corresponds to the value of the mean transition time given in Table 2. These disks diffuse freely only until they collide with one another. When the collision occurs, local concentration of sphingomyelin increases favoring transient formation of a larger domain. Lifetime of the domain would then correspond to the confinement time of around 30 ms given in the manuscript. Fraction of time that the disks spend diffusing freely and trapped in the domain is given by the ratio between the confinement time and the average inter-collision time.

To calculate the collision frequency $f$ and the mean time between two collisions, model proposed by Hardt[10] was applied:

$$f = 2\pi N_{av} c^2 D \frac{1}{\ln\left[ (\pi N_{av} c)^{-1/2} / a \right]}, \qquad \text{Eq. 15}$$

where $N_{av}$ is Avogadro constant, $a$ stays for an encounter radius, which is assumed to be the double of the disk radius (i.e. 10 nm), and $c$ is surface concentration of the disks. The concentration was obtained from the z-scan FCS experiment and the parabolic dependence of the number of particles on the membrane position (Eq. 4). The collision rates and the inter-collision times for the CTxB-647 low and high loaded membrane are

given in Table S3.

| | *N* | *c* | *f* | number of collisions in focus | mean intercollision time |
|---|---|---|---|---|---|
| | | [mol/m$^2$] | [mol/m$^2$s$^{-1}$] | [s$^{-1}$] | [ms] |
| **B**-low load | 0.2 | 1.7E-12 | 7.0E-12 | 0.8 | 778 |
| **B**-high load | 4 | 3.4E-11 | 4.5E-09 | 527.1 | 31 |

Table S3. Theoretical collision parameters for CTxB-647-crosslinked GM1 in the membrane composed of lipid mixture **B**.

The observed concentration dependence of the diffusion law might result from the fact that at high crosslinker concentration, the protein-lipid disks collide more frequently and thus spend considerably longer time trapped in the domains than in the low concentration case.

**References**


(1) Benda, A.; Benes, M.; Marecek, V.; Lhotsky, A.; Hermens, W. T.; Hof, M. *Langmuir* **2003**, *19*, 4120-4126.

(2) Palmer, A. G.; Thompson, N. L. *Appl Optics* **1989**, *28*, 1214-1220.

(3) Wawrezinieck, L.; Rigneault, H.; Marguet, D.; Lenne, P. F. *Biophys J* **2005**, *89*, 4029-4042.

(4) Humpolickova, J.; Gielen, E.; Benda, A.; Fagulova, V.; Vercammen, J.; Vandeven, M.; Hof, M.; Ameloot, M.; Engelborghs, Y. *Biophys J* **2006**, *91*, L23-L25.

(5) Digman, M. A.; Caiolfa, V. R.; Zamai, M.; Gratton, E. *Biophys J* **2008**, *94*, L14-L16.

(6) Baumann, J.; Fayer, M. D. *J Chem Phys* **1986**, *85*, 4087-4107.

(7) Johansson, L. B. A.; Engstrom, S.; Lindberg, M. *J Chem Phys* **1992**, *96*, 3844-3856.

(8) Bergenstahl, B. A.; Stenius, P. *J Phys Chem* **1987**, *91*, 5944-5948.

(9) Margineanu, A., J. I. Hotta, R. A. L. Vallee, M. Van der Auweraer, M. Ameloot, A. Stefan, D. Beljonne, Y. Engelborghs, A. Herrmann, K. Mullen, F. C. De Schryver, and J. Hofkens. 2008. Visualization of membrane rafts using a perylene monoimide derivative and fluorescence lifetime imaging. (vol 93, pg 2877, 2007). *Biophys J* 94:715–715.

(10) Hardt, S. L. *Biophys Chem* **1979**, *10*, 239-243.